

## PIV Measurements of the Flow Field inside an Enclosed Cubical Cavity in Natural Convection

M.A.H. Mamun, D.A. Johnson, K.G.T. Hollands

Department of Mechanical Engineering

University of Waterloo

Ontario, Canada

Email: [da3johns@uwaterloo.ca](mailto:da3johns@uwaterloo.ca)

W.H. Leong

Department of Mechanical and Industrial Engineering

Ryerson University

Toronto, Ontario

Canada M5B 2K3

### Abstract

The natural convection heat transfer across and velocity field in an air-filled cubical cavity with two opposing isothermal faces and the remaining four sides having a linear temperature rise from the cold-face to the hot-face have been measured at different orientations and Ra numbers. Two components of the velocity vectors at the mid-plane inside the cavity have been measured by using Particle Image Velocimetry (PIV) at Ra numbers of  $10^6$  and  $6 \times 10^6$  at each of four different orientations: heating-from-the-side, heating-from-below, singly-inclined, and the diamond orientation. The 95% confidence limit uncertainties in the measured velocity vectors are about 2%. The accuracy and integrity of the experiments were validated by the comparison to some well established CFD results at the heating-from-the-side orientation. It was concluded that the experimental method is sound and so findings at other orientations and at other values of Ra should have an accuracy consistent with the findings of the uncertainty analysis. Therefore, the other results can be confidently used as benchmark data for testing CFD codes. The turbulence intensities at the mid-plane are also presented for all the four orientations and at each Ra number.

## Introduction

Natural convection in differentially-heated cavities has been studied extensively both experimentally and numerically because of its many applications in different fields of science and technology. Many studies have emphasized the heat transfer aspects of the problem, while others have concentrated on the fluid mechanical aspects. These two aspects are in fact closely related, because the rate of the heat transfer depends on the flow structure and vice-versa. The internal natural convection or cavity problem is interesting not only because of the strong coupling between the flow and heat transfer (Ostrach 1988); the sensitivity to the cavity configuration and the thermal boundary conditions imposed at the walls (Elsherbiny et al. 1982) also play important and interesting roles. It was pointed out by Ostrach (1968) that internal natural convection flows (such as those occurring inside a cubical cavity) are considerably more complex than external ones (such as occur when a body is heated in extensive surroundings) even when the geometry of the cavity is relatively simple. Among the various cavity shapes, the cuboidal cavity has been studied most often, because of its simple geometry, its suitability for the validation of CFD codes, and its many engineering applications. These applications include those in solar collector cavities, in airflow in rooms and other building components (such as wall-cavities and double-pane windows), in furnaces, in nuclear reactors, and in the cooling of electronic equipment. The main motivation of the present work is providing experimental data suitable for the validation of CFD codes. As is the case for all such cavities, the buoyancy force drives the fluid motion in the cuboidal cavity. Fluid close to the hot face will be at higher temperature than fluid close to the cold face, causing density variations. Hot fluid will tend to move up, and the cold fluid will tend to fall down. In this way natural convection will occur inside the cuboidal cavity. When the density gradient is normal to the gravity vector, the flow is called "side-heating convection", and it takes place for any magnitude of the density gradient. When the density gradient is parallel but opposed to the gravity vector, the situation is called "heating-from-below convection" or "Rayleigh-Benard type convection", and the flow starts only when a critical density gradient is exceeded. More complex flows will occur when the gravity vector is oblique to the density gradient (i.e. at different orientations of the cuboidal cavity). Very recently a benchmark experimental study for providing data suitable for validating CFD codes was reported by Leong et al. (1998,1999) and Mamun (2003). They investigated natural convection heat transfer in a cubical air-filled cavity with two opposing isothermal faces and the remaining four sides (called the side-walls) having a linear temperature variation from the cold face temperature to the hot face temperature as shown in Figure 1 (also called the "perfectly-conducting" side-wall boundary condition). Three orientations of the cubical cavity were studied: one, called here "heating-from-the-side" had  $\theta=90^\circ$  and  $\phi=0$ ; another, called here "heating-from-below" orientation, had  $\theta=0$  and  $\phi=0$ ; while the third, called here the "singly-inclined" orientation, had the hot and cold faces inclined at  $45^\circ$  (i.e.  $\theta=45^\circ$  and  $\phi=0^\circ$ ). Their study provided precise (1.2% accuracy) measurements of the average Nusselt number, Nu, at the cold face for Rayleigh number, Ra, equal to  $10^4, 4 \times 10^4, 10^5, 10^6, 10^7$  and  $10^8$ .

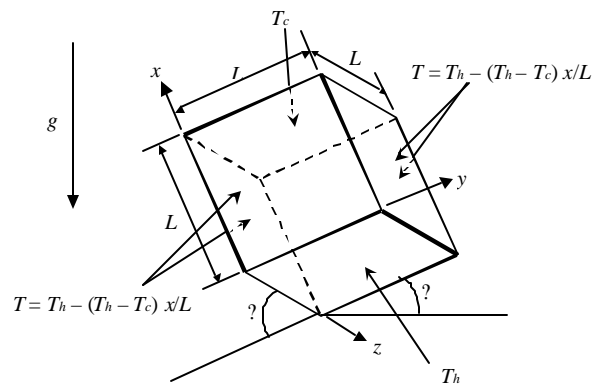


**Figure 1 Cuboidal Cavity**

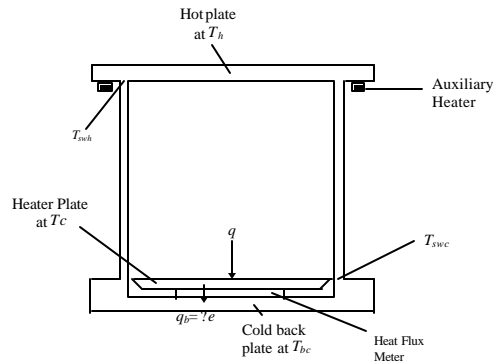
The problem defined by Leong et al. was selected as a validation exercise for the ICHMT 2nd International Symposium on Advances in Computational Heat Transfer, which took place in 2001. Here, validation attempts were made by ten sets of workers (e.g., Krepper(2001), Kenjeres(2001), Pallares(2001)), and the findings of all these attempts were summarized by Pepper and Hollands (2001,2002). Some of these various numerical results matched the experimental values within experimental uncertainty. On the other hand, not one set of worker's results suitably matched the entire set of measured Nu values, despite the diversity of numerical approaches. This high degree of interest and incomplete CFD confirmations indicate that work in this area still needs to be done, and they suggest that an extension providing velocity data is justified. For this reason, the velocity field inside the enclosed cavity was measured, using the particle image velocimetry (PIV) technique. Two components of the velocity vectors at the  $z=W/2$  plane inside the cavity were measured at different orientations, at Ra number  $10^6$  and  $6*10^6$ . At the heating-from-the-side orientation, the flow at Ra number  $10^6$  is known to be laminar, but for the other orientations, turbulence may exist at these Ra, so both the mean values and the rms values are presented for the other orientations. The experimental results for heating-from-the-side orientation at Ra number  $10^6$  were found to be very close to the numerical results of Krepper (2001). Therefore, the other results can be confidently used as benchmark data for comparison with CFD codes.

A large number of experimental, theoretical and numerical studies have been carried out to understand the natural convection heat transfer and flow structure in cuboidal cavities. Ostrach (1988,1982), Catton (1978), Churchill (1983), Raithby and Hollands (1997), Hoogendoorn (1986) and Yang (1987,1988) provided very good reviews, covering the earlier work in this area. Quantitative measurement of the temperature and velocity fields for transient natural convection was conducted in a rectangular cavity of aspect ratio  $H/L=1$  and  $W/L=2$  by Upton and Watt (1997) for  $Pr=6.38$ ,  $Ra=1.5*10^8$  at three inclination angles (i.e.  $\theta=45,90,135$  with  $\theta=0$ ). Particle image velocimetry (DPIV) was used for the velocities although the inclined side-walls were made of acrylic and glass. Tian and Karayiannis (2000) measured the velocity and temperature distribution at different locations in an air filled square cavity at the heating-from-the-side orientation at  $Ra=1.58*10^9$ , using a 2-D laser Doppler anemometer (LDA) and small E-type thermocouples. The side-walls were made of steel plate which gave significant variations from the ideal linear temperature profile as well as from the adiabatic side-wall. Despite these variations the authors recommended using their measured temperature profile as a boundary condition for CFD comparisons. Hiller et al. (1993) used PIV to measure transient natural convection in a cubical cavity. They identified the possible sources of measurement discrepancy as the non-ideal experimental conditions. Pallares et al. (2001) conducted flow visualization and velocity field measurement by PIV in a cubical cavity with acrylic and polycarbonate side-walls. A PIV system using an optical fiber bundle scope was developed and presented by Tani et al. (2000) although the resolution of particle images was found to be poorer than those taken directly by a CCD camera. Velocity and temperature fields in natural convection flow were measured by Meyer et al. (2002), using PIV and Planar-LIF in a cubical cavity with a heated square plate centered in the bottom face, cold side-walls and the remaining walls insulated. All the previous experimental studies for heat transfer, temperature field measurements, flow visualization and quantitative measurement of the flow field are limited to certain orientations and certain ranges of Ra. It was found that all the flow-visualization and velocity field measurement work used glazed side-walls for which there will be heat losses at the side-wall. These imperfect thermal boundary conditions on the side-walls will cause differences between any numerical results and experimental measurements. The differences will be more when the working fluids are gases or low conductivity fluids in moderate aspect ratios (Lepeutre, 1990). The effect of thermal boundary conditions was discussed qualitatively by ElSherbiny et al.(1982). They emphasized the reporting of all the parameters representing the interaction of wall conduction and fluid convection. Although many of the investigators identified such errors in their experimental results, it is still difficult to compare numerical and experimental solutions. A velocity measurement technique is needed that can be done without disturbing the prescribed boundary conditions at the side-walls.

#### Experimental Benchmark Problem

The experiments reported here used the identical air-filled cubical cavity as had been used by Leong et al. (1998) with minor modifications to accommodate the PIV measurements. A cross-sectional view of the cavity in the heating-from-above orientation is shown in Figure 2. The hotplate, cold back plate, heater plate and side-walls were made of copper in order to achieve, respectively, uniform temperatures at the hot

plate, cold back plate, and heater plate, as well as linear temperature distribution along the side-walls. The experimental cube had side length  $L$  nominally equal to 127 mm. It contained a heat flux meter, an electrically heated plate, and two identical hemi-cubes, the latter joining along a parting-line to form the cube after assembly. Heating and cooling was achieved using temperature controlled water streams passing through tubes soldered to the rear faces.



$q = q_b + q_e$   
 $q =$  Total heat transfer (convection, conduction and radiation) from hot plate to cold plate  
 $q_b = ? e =$  Heat flow from the electrically heated heater plate and to the back plate  
 $q_e = VI =$  Electrical power delivered to the heater plate

**Figure 2 Layout of the experimental model**

### Velocity Measurements

### PIV Technique and Implementation

Smoke generated by burning mosquito repellent was used as the seeding particles, as was used by Tian and Karayiannis (2000). A dual cavity Nd:YAG laser with a cylindrical lens was used to make a pulsed light sheet to illuminate the flow. For the purpose of the present study, two very small pieces of a side-wall were redesigned for laser light admission at the  $z=L/2$  plane of the experimental model.

### Image Acquisition

A boroscope with a large field of view was chosen to take the image of the middle illuminated plane. The diameter of the boroscope had to be kept small to minimize the disturbance of the thermal boundary conditions. Four 10 mm diameter holes were drilled into one of the two side-walls that are parallel to the illuminated plane. These holes were used to hold the boroscope end, as shown in Figure 3. The side-wall at  $z=0$  was chosen for this purpose, and Figure 3 shows the locations of the four holes.

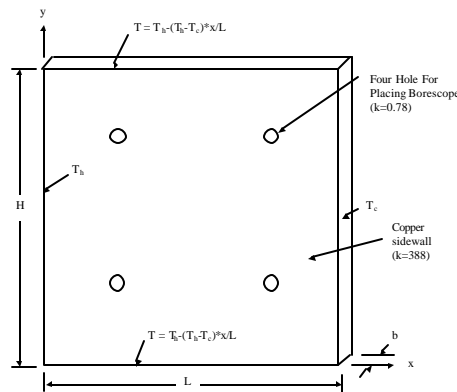


**Figure 3 Dimensions of one piece of side-wall with four holes for the borecope**

The boroscope was placed in each hole, in succession, and the other holes were blocked by a copper plug when not in use. An image from each hole produced greater than a one quarter image of the illuminated cavity plane. A variable focus C-mount 28mm focal length CCF28 coupler was used to connect the boroscope to the CCD camera (Kodak Megaplus ES.1.0, 1008 times 1018 pixel resolution). The laser and the CCD camera were synchronized via a Dantec PIV processor to collect and store the data. When the flow reached steady state, the images were taken through the four holes, one by one, and in this way the whole image of the middle plane of the cubical cavity was taken.

As mentioned earlier, four holes were drilled in one of the side-walls for image acquisition. This caused the required linear distribution to be locally disturbed. A thermal analysis of the side-wall was made assuming a copper wall with four holes, with one hole filled with low conductivity material and other three filled with copper. It showed that the maximum deviation from the linear temperature profile caused by the low conductivity material was 0.40 K for  $\Delta T=10$  K. But the root mean square deviation from the linear temperature profile along the centre line of the holes from hot face to cold face was found to be only 0.11 K. The root mean square deviation from the linear temperature profile for the whole side-wall from hot face to cold face was found to be only 0.07 K. This was considered a small enough deviation to not cause substantial deviations in the flow field. The temperature distribution along the side-wall with the boroscope was measured in the experiment. Results showed that the maximum deviation from the linear temperature profile caused by the boroscope is 0.15 K. This experiment showed the practicality of the analysis and this deviation can be considered small enough to consider the temperature profile linear along the side-wall.

#### Correction of Distortion of Image

Because of the large field of view of the boroscope and small distance of the object plane from its lens, there must be some distortion of the acquired images, and so it is necessary to modify the image recorded on the camera to remove this distortion. A mapping function (a third order polynomial) was used to shift all pixel positions radially. The uncertainty of the 95% confidence limit for this distortion was estimated to be lower than 1% in this application, at position  $x=4.24$  mm and  $y=63.5$  mm.

#### Vector Processing

After the correction of image distortion, the interrogation areas from each image frame are cross-correlated with each other, using  $64 \times 64$  pixel interrogation areas. The above procedure was completed using a fast Fourier Transform-based, cross-correlation algorithm of Gilbert (2003).

#### Measurement Procedure

Experiments were done at two different values of  $Re$ , namely  $10^6$  and  $6 \times 10^6$  for each orientation. The nominal temperatures of hot face and cold face for each  $Re$  were set by adjusting the temperature settings of the constant temperature baths. The electrical power to the auxiliary heater was adjusted until the temperature difference between the hot end of the side-wall and the hot face was less than 0.025 K. The electrical power to the heater plate was adjusted by the computer until the temperature of the heater plate (i.e. cold face),  $T_c$ , was equal to the temperature of the side-walls at the contact to the cold back plate,  $T_{swc}$ , using a feedback loop of the emf output from the HFM and the temperature difference measured by two thermopiles (Leong, 1996).

Following that, the smoke was injected into the cubical cavity. After a 45 min. waiting period the laser light was turned on to produce a light sheet at the middle of the cavity. A total of five hundred pairs of images were recorded for each of the experiments over a time period of about 30 minutes. The necessary measurements such as the emf from the HFM, heater plate power, temperatures of the hot face and cold face, and atmospheric pressure from the barometer in the lab were taken. The variations in each measurement were recorded to determine the "fluctuation intensity" associated with each. The above procedure was repeated by placing the boroscope on each of the remaining three other holes of the side-wall. Further experimental details can be found in Mamun (2003a) and Leong (1996).

#### Method of Analysis

The temperatures of the hot face,  $T_h$ , the cold face,  $T_c$ , the atmospheric pressure,  $P$ , were used to determine the Rayleigh number, in the same way as  $Ra$  was determined in the heat transfer measurement as described in Mamun (2003a) and Leong (1996). Once the 500 pairs of images had been recorded for one orientation of the cavity for one  $Ra$  from one hole of the side-wall, then the data was processed, first to correct for the distortion of the images, and then the vector processing to yield the velocity field.

#### Results and Discussions : Velocity Field

This section presents the velocity measurement results at the  $Z=0.5$  plane inside the cubical cavity for four different orientations at  $Ra$  number  $10^6$  and  $6 \times 10^6$ . The results at  $Ra=10^6$  and one orientation were compared to a well established numerical results as a check on the accuracy and integrity of the experiments.

#### Preliminary Considerations

All the velocities reported here have been non-dimensionalized by division by the reference velocity  $U_r = \sqrt{g \beta (T_h - T_c) L}$ . The value of  $U_r$  was 0.145 m/s for the experiments at  $Ra$  number equal to  $10^6$ , and 0.378 m/s for the experiments at  $Ra$  number equal to  $6 \times 10^6$ .

The measured velocity data have two mean velocities,  $u^*$  and  $v^*$ , and two standard deviations,  $u_{rms}^*$  and  $v_{rms}^*$ , from which the turbulence intensities will be determined. For each orientation and  $Ra$  number combination, the velocity field was measured through each of the four holes on the side-wall, one by one. The total field was established by merging these four sub-fields.

#### Validation of Experimental Method

Usually, CFD codes are validated by comparing them to experimental results of high accuracy. But sometimes the experimental results can be validated by comparison to well developed CFD results in which one has a high degree of confidence. Then, if the experimental results are in good agreement with these CFD results, the experimental results for other cases can be used for validation of CFD codes.

For example, consider the heating-from-the-side orientation at  $Ra=10^6$ , which is a relatively non-challenging situation for a good CFD code. Leong et al. (1999) measured the corresponding Nusselt number within an accuracy of around 1%, and Krepper (2001) checked his numerical results for the Nusselt number against the work of Leong et al. He obtained a result within the uncertainty limits of the result of Leong et al. So now, for this same case, Krepper's velocity field data can be considered as standard data for the validation of the present experimental data of the velocity field at the  $Z=0.5$  plane inside the cavity.

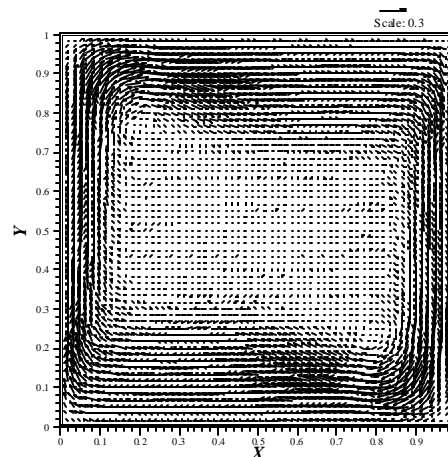


**Figure 4 Measured velocity vectors at the  $Z=0.5$  plane HFS  $Ra 10^6$**

The measured mean velocity vectors at the  $Z=0.5$  p plane inside the cavity in the heating-from-the-side orientation for  $Ra=10^6$  is shown in Figure 4. The rms deviations of the mean velocity field were found to be very small (of order 1%) and this could be attributed to experimental error. Thus the field was found to be laminar, and this is consistent with Krepper's findings. Some of the mean vertical velocity profiles, together with their limits of uncertainty, at different heights in the cavity and the corresponding numerical simulations of Krepper are plotted in Figure 5 allowing direct comparison. The comparison shows generally good agreement. Almost all of the points are within the uncertainty limits of the experimental data. A similar comparison for the mean horizontal velocity profile at  $X=0.5$  is presented in Figure 6. This comparison also shows generally good agreement.

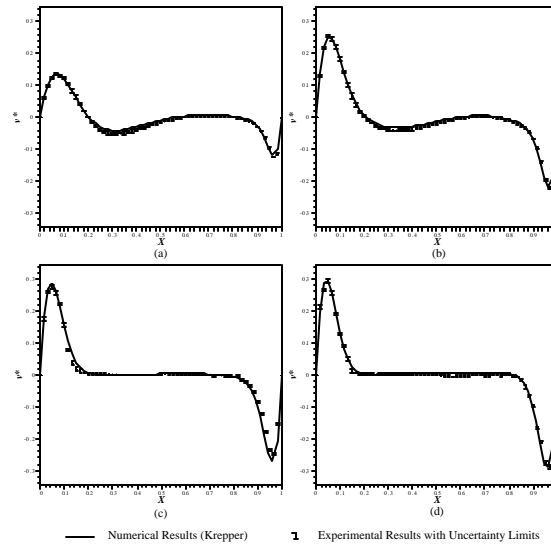


**Figure 5 Vertical velocity profiles at different heights of the cubical cavity for heating-from-the-side orientation at  $Ra=10^6$ : (a) at  $Y=0.4$ , (b) at  $Y=0.3$ , (c) at  $Y=0.2$ , (d) at  $Y=0.1$**

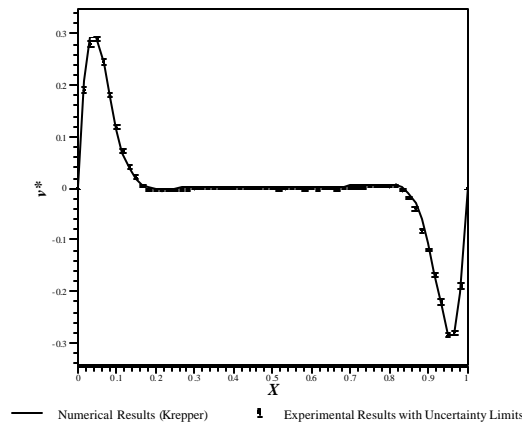


**Figure 6 Horizontal velocity profile at  $X=0.5$  of the cubical cavity for heating-from-the-side orientation at  $Ra=10^6$**

Figure 7 shows the scatter diagram of Krepper's predicted vertical velocity against the measured mean vertical velocity for all four sub-fields, with the limits of uncertainty also shown. There are total 3721 data points in the velocity field and 3471, or around 93%, are within the uncertainty band.

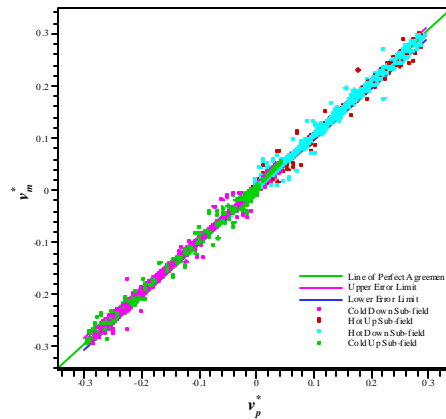


**Figure 7 Scatter diagram of measured vertical velocity vs. predicted vertical velocity**

It is concluded that the experimental method is sound, and so findings at other orientations and at the other Ra number should have an accuracy consistent with the findings of the uncertainty analysis.

#### Determination of Fluctuation Intensity

For the heating-from-the-side orientation at  $Ra=10^6$ , the rms deviations of the velocity vectors were found to be very small (of order 1%), and this could be attributed to the random component of the experimental error.

#### Heating-from-the-side

The mean velocity vectors at the  $Z=0.5$  plane inside the cubical cavity for  $Ra=10^6$  in Figure 5 shows that along the hot face, the fluid flows up, and along the cold face it flows down. The flow leaves the hot face for the cold face along the top horizontal side-wall, and the reverse happens along the horizontal side-wall at the lower part of the cavity. A large velocity gradient occurs near all the faces and walls, but particularly at the hot and cold faces. There are secondary roll cells near two of the corners: one at the top of the hot face and one at the bottom of the cold face. The horizontal boundary layers carry on from the vertical boundary layers and pass between the side-walls and secondary rolls. The secondary roll appears to take fluid away from the side-wall and to make the horizontal layer thick.

The mean vertical velocity profiles show that the vertical velocities are highest near the hot and cold faces, and a peak velocity position occurs closer to the cold and hot face near the mid height of the cavity. The horizontal velocity components are very much smaller than the vertical velocity components near the hot and cold faces. At the mid-height of the cavity the boundary layer on the hot face is anti-symmetrical to that on the cold face. The boundary layers are narrow at the bottom of the hot face and at the top of the cold face and wider at the top of the hot face and at the bottom of the cold face. The flow pattern along the mid-height and mid-length across the cavity are both important in the description of the flow structure in the cavity. The horizontal velocity profile at  $X=0.5$  of the cavity shows that the variation of the horizontal velocity occurs more at the top and bottom part of the cavity. The vertical velocity variation occurs earlier the cold and hot faces. Over the remaining parts of the cavity, there is very small variation of velocities, and the air in the middle of the cavity remains stationary.

The mean velocity vectors at the  $Z=0.5$  plane inside the cubical cavity for  $Ra=6 \times 10^6$  are similar to that at  $Ra=10^6$ . The results show that vertical velocities are higher than that of  $Ra=10^6$  and the boundary layers along the hot and cold face are thinner.

#### Heating-from-below

From the literature for the cubical cavity with perfectly -conducting side-walls, the value of  $Ra_{c1}$  is 6974 (Davis (1967), Catton(1970), while  $Ra_{c2}$  is approx  $4 \times 10^5$  (Xia (2002)), and also the transition from time dependent flow to turbulent flow might occurs in the range of Ra number  $4 \times 10^5$  to  $4.9 \times 10^5$  (Xia, 2002).

The present experiments involve Ra numbers of  $10^6$  and  $6 \times 10^6$ , and can thus be expected to be in turbulent conditions, and this was confirmed by these experiments. Thus at  $Ra=10^6$  it was found that the excess average relative rms values of the velocity components,  $s_u$  and  $s_v$ , are about 95% of  $u^*$  and 100% of  $v^*$ , respectively, indicating that the flow has large fluctuation intensities.

The mean velocity vectors at the  $Z=0.5$  plane for  $Ra=10^6$  are shown in Figure 8. The flow can be interpreted as a combination of four rolls. On the hot face side of the cavity, the fluid flows with a central descending current from the centre of the cavity toward the hot face, and an ascending motion near the side-walls. On the cold face side, the fluid flows with a central ascending current from the centre of the cavity toward the cold face, and a descending motion near the side-walls. A large velocity gradient occurs near all the faces and side-walls and also in the central part of the cavity near the roll cells, at about one-quarter and three-quarters up the cavity. Qualitatively, the flow pattern is similar to that predicted by Krepper (2001) and Pallares et al. (2002). It is clear from Figure 8 that, for example on the hot face side, there is more flow descending toward the central part of the hot face than the flow ascending away at both ends of the hot face near the side-walls. This indicates that a very substantial amount of flow has to come from the third dimension, i.e. the Z direction, in order to satisfy continuity. This was checked by integrating along a line of  $X=0.1$  and the difference is  $-0.002 \text{ m}^3/\text{s}$ . Hence by nature the flow in the heating-from-below orientation is fully three-dimensional.

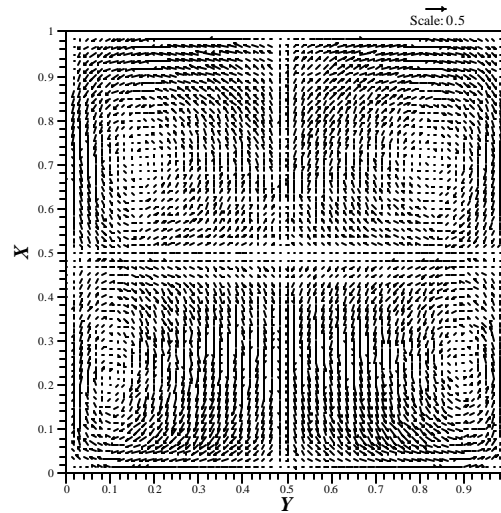


**Figure 8 Mean velocity vectors at the  $Z=0.5$  plane inside the cavity at  $Ra=10^6$  for the heating-from-below orientation**

Some of the mean vertical velocity profiles, together with their limits of uncertainty, at different X positions of the cavity are plotted in Figure 9. These figures show that at each X position the magnitude of the mean vertical velocity is high very close to the side-walls, but it has to be zero at the side-walls, so there are very high velocity gradients near the side-walls. The magnitude of the mean vertical velocity is also high in the central part between the roll cells, but it decreases rapidly near the roll cells resulting in high velocity gradients. The mean vertical velocity profile is symmetrical about central axis at  $Y=0.5$ . The mean vertical velocity is very small at  $X=0.5$  because it is mainly horizontal velocity at this position, and consequently it is not plotted. The mean horizontal velocity profiles with their limits of uncertainty at different Y position of the cavity are presented in Figure 10. These figures show that the magnitude of the mean horizontal velocity is high very close to the hot face and the cold face; but since it is zero at the side-walls, there are very high velocity gradients near the hot face and the cold face. The magnitude of the mean horizontal velocity is also high in the central part at around  $X=0.5$ . The mean horizontal velocity profile is

symmetrical about the central axis at  $X=0.5$ . The mean horizontal velocity is very small at  $Y=0.5$ , and it is not plotted.

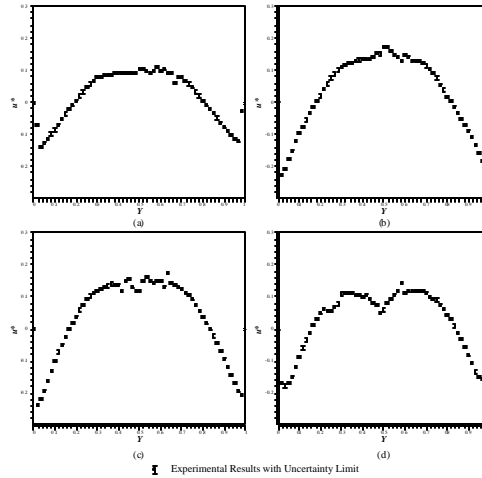


**Figure 9 Mean vertical velocity profile at different X positions of the cubical cavity for the heating-from-below orientation at  $Ra=10^6$  (a) at  $X=0.9$ , (b) at  $X=0.8$ , (c) at  $X=0.7$ , (d) at  $X=0.6$ .**

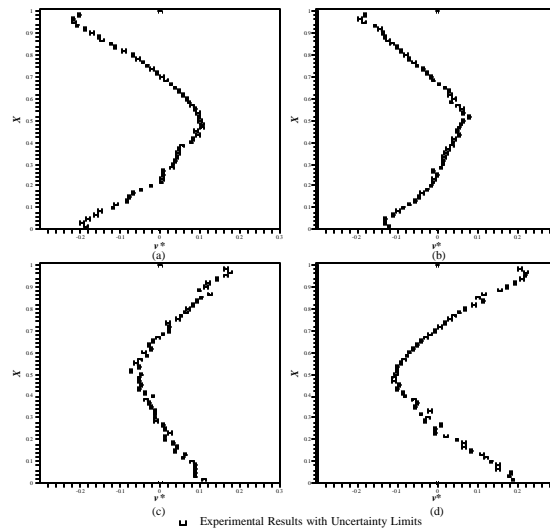


**Figure 10 Mean horizontal velocity profile at different Y positions of the cubical cavity for the heating-from-below orientation at  $Ra=10^6$ : (a) at  $Y=0.2$  (b) at  $Y=0.4$  (c) at  $Y=0.6$ , (d) at  $Y=0.8$**

Similarly the mean velocity vectors at the  $Z=0.5$  plane inside the cavity at  $Ra=6 \times 10^6$  show a flow structure that is similar to that at  $Ra=10^6$ . The four roll cells have moved further towards the corners of the cavity, compared to the situation at  $10^6$ . The excess average relative rms values of the velocity components,  $s_u$  and  $s_v$ , are about 110% of  $u^*$  and 115% of  $v^*$ , respectively, a slight increase in fluctuation intensity over the  $Ra=10^6$  case.

### Conclusion

The natural convection heat transfer and the flow field in an air-filled cubical cavity with two opposing faces being differentially heated and four side-walls with linear temperature variation from hot face to cold face has been measured at different orientations and  $Ra$  numbers. Due to the experimental design

appropriate temperature boundary conditions were obtained which still allowed access to the cavity for velocity measurements.

Two components of the velocity vectors and their fluctuation components at the mid-plane have been measured at Ra numbers of  $10^6$  and  $6 \times 10^6$  at each of the four different orientations: heating-from-the-side, heating-from-below, singly-inclined, and the diamond orientation. The experiments were conducted using the PIV technique, and had high accuracy, with the 95% confidence limit uncertainties in the measured velocity vectors being around 2%. The accuracy and integrity of the experiments were validated by comparing the results at  $Ra=10^6$  and at the heating-from-the-side orientation to the well-established CFD results of Krepper (2001). Therefore, the other results can be confidently used as benchmark data for comparison with CFD code predictions.

The average relative rms values of the velocity components,  $s_u$  and  $s_v$  were calculated from the fluctuating components of the mean velocities. For the heating-from-the-side orientation at Ra number  $10^6$ , the rms deviations of the velocity fields were found to be very small, of order 1%, and this could be attributed to the random component of the experimental errors. But for the other cases, turbulence exists, so the rms values are presented as part of the results.

For the heating-from-the-side orientation at both Ra numbers of  $10^6$  and  $6 \times 10^6$ , sharp velocity changes occur near the cold and hot faces and the side-walls, but at the centre of the cavity the fluid is almost stationary. Also, there are secondary roll cells near two of the corners: the corner at the top of the hot face and the corner at the bottom of the cold face. In this Ra number range the average relative rms values of the velocity components varies from 1% to 2%.

In general for each orientation as the Ra number increases from  $10^6$  to  $6 \times 10^6$ , the velocities increase, the boundary layers near the plates and side-walls become thinner, the rms value of velocities increase, and the secondary cells, where present, move closer to the corners of the cavity.

## References

- I. Catton, 1970, "Convection in a closed rectangular region: The onset of motion," *Journal of Heat Transfer*, vol. 92, pp. 186-187.
- I. Catton, 1978, "Natural convection in enclosures," in *Proceeding of the Sixth International Heat Transfer Conference*, vol.6, pp. 13-31.
- S.W. Churchill, 1983, *Free Convection in Layers and Enclosures*, *Heat Exchanger Design Handbook*, Edited by E.U. Schlunder et.al., Chapter 2.5.8, Hemisphere, Washington, DC.
- S.H. Davis, 1967, "Convection in a box: linear theory," *Journal of Fluid Mechanics*, vol. 30, pp. 465-478.
- S.M. ElSherbiny, K.G.T. Hollands, and G.D. Raithby, 1982, "Heat transfer by natural convection across vertical and inclined air layers," *Journal of Heat Transfer*, vol. 104, pp.96-102.
- S.M. ElSherbiny, K.G.T. Hollands, and G.D. Raithby, 1983, "Nusselt number distribution in vertical and inclined air layers," *Journal of Heat Transfer*, vol. 105, pp. 406-408.
- S.M. ElSherbiny, K.G.T. Hollands, and G.D. Raithby, 1982, "Effect of thermal boundary condition on natural convection in vertical and inclined air layers," *Journal of Heat Transfer*, vol. 104, pp. 515-520.
- R. Gilbert, D.A. Johnson, 2003, "Evaluation of FFT-based cross-correlation algorithms for PIV in a periodic grooved channel," *Experiments in Fluids*, vol. 34, pp. 473-483.
- W.J. Hiller, S. Koch, T.A. Kowalewski, and F. Stella, 1993, "Onset of natural convection in a cube", *International Journal of Heat and Mass Transfer*, vol. 36, pp. 3251-3263.

- C.J. Hoogendoorn, 1986, "Natural convection in enclosures," in Proceeding of the Eight International Heat Transfer Conference, vol. 1, pp. 111-120.
- S. Kenjeres, S.B. Gunarjo, and K. Hanjalic, 2001, "Natural convection in an air-filled cubical cavity under different angles of inclination: a benchmark study," in Proceedings of 2<sup>nd</sup> International Symposium on Advances in Computational Heat Transfer, ICHMT, Palm Cove, Queensland, Australia, May 20-25.
- E. Krepper, 2001, "CHT'01: Validation exercise: natural convection in an air-filled cubical cavity," in proceedings of 2<sup>nd</sup> International Symposium on Advances in Computational Heat Transfer, ICHMT, Palm Cove, Queensland, Australia, May 20-25.
- W.H. Leong, K.G.T. Hollands, and A.P. Brunger, 1998, "On a physically-realizable benchmark problem in the internal natural convection," International Journal of Heat and Mass Transfer, vol. 41, pp. 3817-3828.
- W.H. Leong, K.G.T. Hollands, and A.P. Brunger, 1999, "Experimental Nusselt Numbers for a Cubical-cavity Benchmark Problem in Natural Convection," International Journal of Heat and Mass Transfer, vol. 42, pp. 1979-1989.
- W.H. Leong, 1996, "Benchmark experiments on natural convection heat transfer across a cubical cavity," Ph.D. Thesis, Department of Mechanical Engineering, University of Waterloo, Waterloo, Ontario, Canada.
- M.A.H. Mamun, W.H. Leong, K.G.T. Hollands, and D.A. Johnson, 2003, "Cubical-Cavity Natural-Convection Benchmark Experiments: an Extension," International Journal of Heat and Mass Transfer, vol. 46, pp. 3655-3660.
- M.A.H. Mamun, 2003, "Natural Convection Heat Transfer and Flow Field inside a Cubical Cavity," Ph.D. Thesis, Department of Mechanical Engineering, University of Waterloo, Waterloo, Ontario, Canada.
- K.E. Meyer, P.S. Larsen, F. Guillard and C.H. Westergaard, 2002, "Temperature and velocity fields in natural convection by PIV and LIF," in Proceeding of 11th Int. Symposium on Application of Laser Technology to Fluid Mechanics, July, Lisbon, Portugal.
- S. Ostrach, 1968, "Completely confined natural convection," in Proceedings of the Tenth Midwestern Mechanics Conference on Development in Mechanics, vol. 4, pp. 53-81.
- S. Ostrach, 1982, "Natural convection heat transfer in cavities and cells," in Proceeding of the Seventh International Heat Transfer Conference, vol. 1, pp. 365-379.
- S. Ostrach, 1988, "Natural convection in enclosures," Journal of Heat Transfer, vol. 110, pp. 1175-1190.
- J. Pallares, I. Cuesta, and F.X. Grau, 2001, "Natural convection in an air-filled cubical cavity contribution to the validation exercise," in Proceedings of 2<sup>nd</sup> International Symposium on Advances in Computational Heat Transfer, ICHMT, Palm Cove, Queensland, Australia, May 20-25.
- J. Pallares, I. Cuesta, and F.X. Grau, 2002, "Laminar and turbulent Rayleigh-Benard convection in a perfectly conducting cubical cavity," International Journal of Heat and Fluid Flow, vol. 23, pp. 346-358.
- D.W. Pepper and K.G.T. Hollands, 2001, "Benchmark summary of numerical studies: 3-D natural convection in air-filled enclosure," in Proceedings of 2<sup>nd</sup> International Symposium on Advances in Computational Heat Transfer, ICHMT, Palm Cove, Queensland, Australia, May 20-25.
- D.W. Pepper and K.G.T. Hollands, 2002, "Benchmark summary of numerical studies: 3-D natural convection in air-filled enclosure," Numerical Heat Transfer, vol. 42, No 1/2, part A, pp. 1-11.
- Y. Le Peutrec and G. Lauriat, 1990, "Effect of the heat transfer at the side walls on natural convection in cavities," Journal of Heat Transfer, vol. 112, pp. 370-378.

G.D. Raithby and K.G.T. Hollands, 1997, Natural Convection, Handbook of Heat Transfer Fundamentals, Chapter 4, pp. 4.1-4.99.

N. Tani, M. Mori, K. Hishida, and M. Maeda, 2000, "Development of fiber-bundle-image-guided PIV," in Proceeding of 10<sup>th</sup> International Symposium on Application of Laser Technology to Fluid Mechanics, July 10-13, Lisbon, Portugal, pp. 1-10.

Y.S. Tian and T.G. Karayiannis, 2000, "Low turbulent natural convection in an air filled square cavity, Part I: The thermal and fluid flow fields," International Journal of Heat and Mass Transfer, vol. 43, pp. 849-866.

T.D. Upton and D.W. Watt, 1997, "Experimental study of transient natural convection in an inclined rectangular enclosure," International Journal of Heat and Mass Transfer, vol. 40, pp. 2679-2690.

C. Xia and J.Y. Murthy, 2002, "Buoyancy-driven flow transitions in deep cavities heated from below," Journal of Heat Transfer, vol. 124, pp. 650-659.

K.T. Yang, 1987, Natural Convection in Enclosures, Handbook of Single-Phase Convective Heat Transfer, Chapter 13.

K.T. Yang, 1988, "Transition and Bifurcation in Laminar Buoyant Flows in Confined Enclosure," Journal of Heat Transfer, Vol. 110, pp. 1191-1204.